

1 **Pacific Sea Surface Temperature and the Winter of 2014**

2

3 Dennis L. Hartmann¹

4

5

6 Corresponding Author: Dennis L. Hartmann, Department of Atmospheric Sciences,
7 Box 351640, University of Washington, Seattle, Washington 98195

8

9 Key Points:

- 10 • SST anomalies in the Pacific were a primary cause of the severe winter of 2014.
11 • Warmth in the tropical west Pacific led to cold in central North America.
12 • Specified SST model experiments replicate the observed teleconnections.

13

¹ Department of Atmospheric Sciences, University of Washington,
Seattle, Washington 98195

14

15 **Abstract** It is shown from historical data and from modeling experiments that a
16 proximate cause of the cold winter in North America in 2013-14 was the pattern of
17 sea surface temperature (SST) in the Pacific Ocean. Each of the three dominant
18 modes of SST variability in the Pacific is connected to the Tropics and has a strong
19 expression in extratropical SST and weather patterns. Beginning in the middle of
20 2013 the third mode of SST variability was two standard deviations positive and has
21 remained so through January of 2015. This pattern is associated with high pressure
22 in the northeast Pacific and low pressure and low surface temperatures over central
23 North America. A large ensemble of model experiments with observed SSTs
24 confirms that SST anomalies contributed to the anomalous winter of 2014.

25

26 Index Terms: 3305 Climate change and variability; 3339 Ocean/Atmosphere
27 Interactions; 4513 Decadal Ocean Variability; 4572 Upper Ocean and Mixed-Layer
28 Processes

29 Keywords: Pacific Decadal Oscillation, North Pacific Mode, El Niño

30

31 **1. Introduction**

32 Much interest has focused on the very cold winter in the central and eastern US and
33 Canada in 2013-14 (hereafter the winter of 2014). It has been suggested that
34 melting of polar sea ice could be responsible for causing unusual weather events
35 ([Francis and Vavrus, 2012] but see [Barnes, 2013]), perhaps through the
36 intermediacy of stratospheric warmings [Kim et al., 2014]. This would be
37 remarkable given the small area of the Arctic Ocean and its presence at the tail end
38 of the atmospheric and oceanic chain moving energy from the Tropics toward the
39 poles. Taking a different perspective, Ding et al. [2014] use models and
40 observations to show that at least some of the recent Arctic warming has been
41 forced by changes in the tropical Pacific. Here the coupled variability between the
42 Pacific Ocean and the global atmosphere is used to account in part for the unusual
43 winter of 2014. Using a combination of analysis of past data and a large ensemble of
44 specified SST modeling experiments, a strong case can be made that variability of
45 the ocean-atmosphere system originating in the Tropics is the most likely “cause” of
46 the winter of 2014 anomalies.

47

48 The ocean provides the long-term memory for the climate system through its higher
49 heat capacity, slowly varying large-scale modes and long adjustment time to
50 changes in forcing. The El Niño Southern Oscillation (ENSO) phenomenon is a
51 coupled ocean-atmosphere phenomenon that is the dominant mode of interannual
52 variability globally, and has provided the opportunity to make useful forecasts of
53 seasonal weather and climate conditions a season or more in advance [Neelin et al.,

54 1998; *Rasmusson and Wallace*, 1983]. ENSO has a related decadal variability, the
55 Pacific Decadal Oscillation (PDO), which was first defined in terms of North Pacific
56 sea surface temperature (SST) anomalies [*Mantua and Hare*, 2002; *Zhang et al.*,
57 1997], and is now thought to influence global mean temperature on decadal time
58 scales [*Huber and Knutti*, 2014; *Kosaka and Xie*, 2013; *Trenberth and Fasullo*, 2013].
59 Interannual anomalies of SST are known to have a significant influence on climate
60 over land, and these relationships play an important role in seasonal climate
61 forecasting [*Palmer and Anderson*, 1994] and in the explanation of drought [*Seager*
62 *and Hoerling*, 2014]. While the connection between tropical SST anomalies and
63 winter weather in the extratropics is well established [*Horel and Wallace*, 1981], SST
64 anomalies in middle latitudes are driven by atmospheric anomalies and it is more
65 difficult to show an influence of extratropical SST anomalies in driving atmospheric
66 anomalies [*Kushnir et al.*, 2002; *Lau and Nath*, 1994]. The extratropical SST
67 anomalies associated with ENSO are caused primarily by atmospheric anomalies
68 propagating from the Tropics [*Alexander et al.*, 2002].

69

70 In this paper we explore anomalies in monthly mean SST in the Pacific and their
71 relation to recent weather anomalies. We first present a decomposition of Pacific
72 Ocean SST variability into three key modes; ENSO, which has its strongest variability
73 on time scales of 2 to 6 years, and two decadal modes that are related to ENSO, and
74 have a strong expression in the North Pacific. We next relate these SST patterns to
75 atmospheric variability and show that one of the decadal modes is associated with
76 atmospheric anomalies that look very much like those during the winter of 2014.

77 This mode of variability showed a positive anomaly of two standard deviations
78 beginning in the summer of 2013. To demonstrate a causality relationship between
79 this large anomaly in the SST mode and the winter of 2014, we analyze a large
80 ensemble of specified-SST modeling experiments. Since these specified-SST
81 experiments produce anomalies with similar structure and amplitude to the
82 observed anomalies in 2014, we conclude that SST variations rooted in the Tropics
83 played a key role in producing the cold winter of 2014.

84

85 **2. SST Variability: ENSO, PDO and North Pacific Mode**

86

87 The Pacific Decadal Oscillation (PDO) has classically been defined as the first
88 Empirical Orthogonal Function (EOF) of the anomalies of monthly mean SST
89 poleward of 20N in the Pacific Ocean [*Mantua et al., 1997*]. Bond et al. [2003] noted
90 that the second EOF of North Pacific SST was anomalously negative in 1999-2002,
91 and emphasized that the PDO alone is not sufficient to characterize the variability of
92 the North Pacific. Here we include the ocean region from 30S-65N and 120E-105W,
93 which includes the tropical and North Pacific. We use the NOAA ERSST data set
94 [*Smith et al., 2008*] to compute the EOF decomposition after removing the seasonal
95 cycle, the global mean and the linear trend from the monthly data. We have
96 obtained similar results with the HadISST data set [*Rayner et al., 2003*] (not shown).
97 Although the data set starts in 1854, we focus on the period since 1900 when the
98 data are more complete. The first EOF expresses about 30% of the variance and the
99 next two modes each express about 8% of the variance (S1). The second and third

100 modes are not distinguished from each other by their explained variance [*North et*
101 *al.*, 1982], and their relative rankings will change for different sampling periods. For
102 example, the third mode for the period from 1900 becomes the second mode in the
103 period since 1979. The remaining EOFs form a continuum of modes that are not
104 distinguished from each other by their explained variance. The SST modes shown
105 here are for all 12 months, but the basic structures are the same if winter or
106 summer half years are used instead. The structures and explained variances are
107 very similar if we use instead only the period since 1950, when the observational
108 network had improved further. The first three SST modes are shown in Fig. 1 as
109 regressions of the SST anomalies with the principal component time series of each
110 mode. The first mode captures much of the equatorial variance, but the second and
111 third modes also have significant connections to the Tropics.

112

113 In the supplementary materials we show that these three modes are related to each
114 other (S2). The second mode tends to become strongly positive after a warm ENSO
115 event. This expresses the fact that the extratropical signature of a warm event,
116 which gives cold SST in midlatitudes via the “atmospheric bridge” [*Lau and Nath,*
117 *1996*], tends to persist longer than ENSO itself. So its structure is cold in
118 midlatitude western Pacific and also cold in the eastern equatorial Pacific. The third
119 mode tends to be in its positive phase prior to ENSO warm events and is closely
120 related to the “footprinting” mechanism [*Vimont et al.*, 2001; *Vimont et al.*, 2003].
121 The structures of the second and third modes in Fig. 1 appear to be dominated by
122 amplitude away from the equator, but they are nonetheless connected to the

123 Tropics. The variance of SST is large in the North Pacific (not shown) so the
124 regressions are large there, but both the correlation patterns associated with these
125 two modes and their strong temporal relationship to ENSO, indicate their tropical
126 roots.

127

128 During the satellite era since 1979, the third mode has been very strong, and it
129 enters as the second mode of global SST during that period (not shown). In the
130 classical analysis of the PDO using the region poleward of 20N [*Mantua and Hare,*
131 2002], the first mode is that identified as the PDO, while the second mode is very
132 similar to the third mode for the larger domains employed here. Deser and
133 Blackmon [1995] referred to the second mode SST structure as the North Pacific
134 Mode (NPM). The NPM mode is very robust to the region used. It appears as the
135 second mode for the Pacific region north of 20N, one of two modes centered in the
136 North Pacific for the Pacific Ocean north of 30S shown here, and also as the second
137 mode of global SST for the period since 1979.

138

139 The extratropical signatures of the second and third modes in Fig. 1 may be
140 influenced by the North Pacific Gyre Oscillation [*Ceballos et al., 2009; Chhak et al.,*
141 2009; *Di Lorenzo et al., 2008*] and by fluctuations in the Kuroshio and Oyashio
142 Currents [*Frankignoul et al., 2011; Kwon et al., 2010*]. Seager et al. [2001]
143 performed an ocean heat budget analysis in the Kuroshio-Oyashio Extension region
144 and showed how surface fluxes, Ekman current-induced ocean heat convergence
145 and Rossby wave adjustment combine to generate the SST anomalies. Thus both

146 atmospheric forcing and the oceanic dynamic response are important for the
147 evolution of the North Pacific SST and surface height (e.g. Miller et al. [1998], Vivier
148 et al. [1999], Qiu [2000], Cummins and Freeland [2007]). Local atmospheric forcing
149 seems to be very important in the North Pacific at least on seasonal and interannual
150 time scales, and both local and remote influences may be important [*Alexander et al.*,
151 2002; *Liu and Alexander*, 2007]. Smirnov et al [2014] conclude that internal ocean
152 dynamics play little role in interannual SST variability in the eastern Pacific in
153 comparison to the western Pacific where the Kuroshio and Oyashio currents may
154 play a more important role.

155

156 The principal components of the first three EOFs are shown in Fig. 2 in units of
157 standard deviations for the period from 1979 to January of 2015. These EOFs are
158 based on the Pacific north of 30S during the period from 1900 to 2014. During the
159 most recent period shown in Fig. 2, hints of the relationships between the three
160 EOFs during warming events can be seen. Both the second and third modes show
161 large amplitude variations associated with major warming events. Since the 1998
162 warm ENSO event the principal components of the first two EOFs have been mostly
163 negative, which is a reflection of the tendency for cool ENSO and negative PDO since
164 then. After May 2013, however, the first two EOFs were near neutral amplitude,
165 while the third EOF (NPM) maintained a positive value near two standard
166 deviations above neutral. Unusually warm temperatures in the northeast Pacific
167 prevailed during this period.

168

169 The very high SST anomaly in the North Pacific that emerged in May of 2013 is
170 linked to reduced cooling of the ocean during the prior winter of 2013. The SST,
171 heat content, surface wind stress and surface heat flux anomalies for 2013 are well
172 illustrated in the State of the Climate – 2013 report [*Blunden and Arndt, 2014*],
173 particularly in Figs. 3.1 to 3.9 [*Newlin and Gregg, 2014*]. These show strongly
174 suppressed wind stresses, and positive anomalies of surface heat fluxes into the
175 North Pacific Ocean during 2013. It is likely that these anomalies are rooted in the
176 Tropics, but it is important to confirm what caused these anomalous fluxes in 2013
177 and to what extent the heat stored then influenced the weather of the following
178 winter.

179

180 **3. Meteorological connections to Pacific SST anomalies**

181

182 We have regressed the monthly principal components of the first three EOFs of SST
183 on the 500hPa height and lowest model level temperature from both the 20th
184 Century Reanalysis that starts in 1871 [*Compo et al., 2011*] and the NCEP/NCAR
185 Reanalysis that starts in 1948 [*Kalnay et al., 1996*]. We obtain similar results from
186 both reanalysis data sets and from shorter subsets of each data set. For the sake of
187 brevity we show the results for the NCEP/NCAR Reanalysis.

188

189 Since the focus of this paper is the influence of the North Pacific Mode on the winter
190 of 2014, we will show only the regression for that mode here, but correlation
191 patterns for all three modes are shown in the supplementary materials (S3). Fig. 3a

192 shows the anomaly of the 500hPa field for November to March of 2013-14, the
193 winter of 2014. It shows a ridge over the North Pacific and a deep trough over the
194 central North American centered just south of Hudson Bay. The northerly flow
195 between these two centers, which is roughly aligned with the Rocky Mountains,
196 brought cold Arctic air into central North America and gave unusually cold
197 conditions there.

198

199 Fig. 3b shows the regression of the global 500hPa height field from NCEP/NCAR
200 reanalysis during months of November through March onto the second principal
201 component of global SST based on the period from 1979. The second mode of global
202 SST for 1979 to 2014 is very similar to the third mode of SST for the period 1900 to
203 2014 shown in Fig. 1. Fig. 3b is not very different when based on the SST since 1900
204 and the NCEP/NCAR data since 1948, but we show the satellite era data to be
205 consistent with the model simulations discussed later. The regressions show the
206 amplitude explained by a one standard deviation variation of the principal
207 component. A large high pressure occurs over the northern Pacific centered near
208 the Aleutian Islands with a downstream low centered near Hudson Bay. These are
209 connected to a low along 30N over the Pacific Ocean.

210

211 Fig. 4 shows the same anomalies and regressions as in Fig. 3, except for the
212 temperature anomalies at the lowest model level. During the winter of 2014
213 extreme cold anomalies persisted across North American while warm anomalies
214 persisted in the Northeast Pacific and in Alaska. These anomalies are also reflected

215 in the regression of the North Pacific Mode of SST onto the low level temperatures in
216 Fig. 4b. The regression shows a maximum cold anomaly of about 1°C over North
217 America for one standard deviation departure of the NPM, so for a two standard
218 deviation of the NPM SST, the regression predicts a surface temperature anomaly of
219 about 2°C over North America, which is close to the 2.6°C anomaly in Fig. 4a.

220

221 The statistical significance of the features in the regression plots shown here is
222 assessed by determining whether the correlations associated with them are
223 different from zero at the 95% level. The degrees of freedom have been determined
224 using the approximation recommended by Bretherton et al. [1999]. Although the
225 SST indices are highly auto-correlated, the extratropical height anomalies are not, so
226 that for the 67-year record from 1948 and the 5 months of November to March, the
227 data used to perform the height regressions possesses about 250 degrees of
228 freedom. For the record since 1979, the degrees of freedom still number 130. With
229 this large number of degrees of freedom, relatively small correlations become
230 significant, and the question shifts to whether the fraction of variance explained is
231 interesting or not. Thus the absolute values of the correlation coefficients are of
232 more interest than their proven statistical significance. The correlation coefficient
233 map corresponding to Figs. 3b and 4b have correlations between 0.3 and 0.4 for the
234 centers over North America. For comparison, the correlations associated with the
235 ENSO mode exceed 0.6 in the extratropics for SST EOFs computed from both the
236 global and Pacific regions. We therefore conclude that the winter of 2014 over

237 North America was favored by the prevailing NPM SST anomaly pattern over the
238 Pacific Ocean.
239

240 Wang et al. [2013] explore the influence of SST modes on North American weather.
241 They estimate that the three leading modes they consider explain about 50% of the
242 total effect of SST on North American Climate, but the modes they considered in the
243 Pacific correspond roughly to the ENSO mode and the PDO mode (or Kuroshio
244 extension mode) and they do not consider the NPM described here. Since our
245 analysis shows that the second and third modes explain the same amount of
246 variance, any linear combination of the two is as valid a representation as either
247 mode alone. Since the third mode reaches large amplitude during the period of
248 interest, while the first and second are near neutral, it is meaningful to consider only
249 the third mode in detail here.
250

251 The pattern of SST and height variability we find with the NPM is similar to the
252 structure that Seager et al. [2014] associate with the California drought, particularly
253 during the Nov.-April 2013-14 period. They used model experiments with specified
254 SST to show that these anomalies are keyed to warm SST anomalies in the tropical
255 Pacific west of the dateline. The ridge-trough pattern over North America
256 suppresses precipitation in California while it also induces cold anomalies in the
257 middle of the continent. We emphasize the cooling effect here. It should be noted
258 that the prior two winters of 2011-12 and 2012-13 were not strong positive NPM
259 years (Fig. 1). The ridge was farther west off shore, and the deep trough over North

260 American was much less developed. The drought during those years was more
261 likely associated with the strong La Niña conditions during the 2011-12 winter, with
262 continued warm SST in the western equatorial Pacific the following year, and the
263 strongly positive NPM mode in 2013-14 completed three years of intense drought in
264 California.

265

266 Similarly, Wang et al [2014] associated the California drought of 2013-14 with the
267 anomaly height pattern for NDJ, which is very similar in structure to Fig. 3. They
268 focused particularly on the dipole pattern between the ridge in the Gulf of Alaska
269 and the trough centered just south of Hudson Bay. They found that this pattern was
270 correlated with the Niño4 SST index, one year prior. In general outline this is
271 consistent with our conclusion that the winter of 2014 pattern is associated with a
272 precursor mode of ENSO. Wang et al. [2014] go on to conclude that this pattern is
273 becoming more prevalent in consequence of human-induced warming of the climate.
274 Seager et al. [2014] conclude that the California drought is largely natural variability
275 and has precedents in earlier times. We do not investigate any connections to
276 climate change in this paper.

277

278 **4. Specified SST Experiments**

279 So far it has been demonstrated that the structure that dominated the winter
280 weather in North America in 2014 is similar in shape and slightly smaller than the
281 regression onto the NPM SST pattern that dominated in that year. To make a
282 stronger case that the SST anomaly caused some important part of the weather

283 anomaly, rather than merely being associated with it, we turn to AMIP-style
284 experiment data provided by the NOAA-ESRL Physical Sciences Division, Boulder,
285 Colorado from their website at
286 <http://www.esrl.noaa.gov/psd/repository/alias/facts/> . The experiments chosen
287 apply the observed radiative forcing and specify the observed SSTs under an
288 atmospheric model. Large ensembles of experiments starting in 1979 were
289 conducted with several different models of the atmosphere. Three model
290 ensembles are considered here; a 50-member ensemble with the ESRL-GFSv2 model,
291 a 30-member ensemble with the ECHAM5 model, and a 20-member ensemble with
292 the CAM4 model. We use the ensemble mean anomalies for each model to both
293 regress them onto the SST indices. To be consistent with our data analysis we
294 remove the linear trend.

295

296 Fig. 3c shows the regression of the 500hPa height anomalies for the ESRL-GFSv2 50-
297 member ensemble mean onto the NPM mode. The ECHAM5 and CAM4 models
298 produce similar results (S5). The predicted anomaly has key features in common
299 with the observed anomaly in Fig. 3a, but with smaller amplitudes. The depth of the
300 low at about 35N in the central Pacific is well simulated, but the ridge on the West
301 Coast and especially the downstream low over North America are much attenuated
302 compared to the observed regression pattern in Fig. 3b.

303

304 Fig. 4c shows the corresponding regression for the simulation of the temperature at
305 the lowest model level. The story is very similar to that for the 500 hPa height. The

306 regression of the simulated temperatures onto the NPM SST mode captures many of
307 the key features of the anomalies of 2013-14, especially the cold conditions over
308 North America. The regression pattern produced by the AMIP simulations has a
309 much weaker cool anomaly over North America than for the regression on
310 observations. It is unclear why the models underestimate the observed connections
311 between SST and North American weather. The model resolution in these
312 experiments is 0.75 to 1 degree, and it is possible that the wave pattern is sensitive
313 to the resolution of the Rocky Mountains, which are smoothed somewhat in these
314 simulations.

315

316 In future work we could look to see if a significant number of the ensemble
317 members do get the observed downstream amplitude in 2014, but that is an
318 additional data processing chore. It is important to remember that fixed SST
319 experiments do not capture the full interaction between the atmosphere and ocean
320 [*Barsugli and Battisti, 1998*], and simple interpretations of ensembles often
321 underestimate the confidence of seasonal predictions [*Eade et al., 2014*]. For the
322 1979 to 2014 period there is little difference between the regression on the global
323 SST pattern, and the NPM pattern for the Pacific north of 30S. Although the winter
324 of 2014 was a two-sigma event in terms of the NPM of SST, the regressions with
325 NCEP/NCAR Reanalysis include 35 (or 67 for the period since 1948) winters and are
326 not very sensitive to the inclusion or not of the winter of 2014.

327

328 **4. Discussion and Conclusion**

329

330 It appears that the sudden increase in the NPM SST anomaly pattern in the North
331 Pacific during the middle of 2013 can be associated with the subsequent cold winter
332 in the center of North America. Although the pattern of SST anomaly is very strong
333 in the North Pacific, it is virtually certain that the forcing for these anomalies
334 originates with warm SST in the tropical west Pacific. Preliminary experiments
335 indicate that the atmospheric pattern during the winter of 2014 is not efficiently
336 forced by the extratropical SST anomalies, but can be generated with the observed
337 warm SST anomalies in the tropical west Pacific (Paulo Ceppi personal
338 communication). This result is consistent with a long history of observational and
339 modeling work indicating that SST anomalies in the extratropics are strongly driven
340 by atmospheric circulation anomalies [*Cayan, 1992; Davis, 1976*], while SST
341 anomalies in the tropics can strongly force the atmospheric circulation [*Lau and*
342 *Nath, 1994*].

343

344 The NPM mode of SST variability remains strongly positive as of this writing in
345 January of 2015, and its future evolution will be interesting to watch. The reasons
346 why the NPM anomalies arose so strongly in the middle of 2013 remain to be
347 explored. The stage was set for the very positive NPM extratropical SST anomaly of
348 the 2014 winter by a reduction in heat extraction from the North Pacific in the prior
349 winter of 2013. The annual mean 500hPa anomaly for 2013 shows a large high
350 pressure over the North Pacific centered at about 50N 150W (not shown).

351 Generally warm anomalies of the SST in the tropical western Pacific have persisted
352 since the winter of 2013 (<http://www.esrl.noaa.gov/psd/map/clim/sst.shtml>).
353
354 Midlatitude seasonal weather and climate anomalies receive a large contribution
355 from internal atmospheric variability that is unrelated to any interactions with the
356 SST (e.g. Deser et al. 2012). The effect of ocean heat anomalies and associated SST
357 anomalies on the seasonal weather patterns can thus be negated by other variability
358 in any particular months. Nonetheless, the systematic connection between NPM SST
359 anomalies and winter weather in the past, the extreme amplitude of the SST
360 anomalies in 2013-14, and the similarity of the 2014 winter anomalies to the
361 historical pattern, all suggest that the warm SST in the tropical and north Pacific
362 likely made a significant contribution to the cold winter in central North America in
363 2013-14. Specified SST simulations with three models confirm the causal
364 relationship between the NPM SST mode and winter weather in North America.
365
366
367 Acknowledgments: The SST data were obtained from the NOAA ERSST data set at
368 <http://www.esrl.noaa.gov/psd/data/gridded/data.noaa.ersst.html>. 20th Century
369 Reanalysis and NCEP/NCAR Reanalysis products were obtained from the NOAA web
370 sites http://www.esrl.noaa.gov/psd/data/20thC_Rean/ and
371 <http://www.esrl.noaa.gov/psd/data/gridded/data.ncep.reanalysis.html>. AMIP simulations
372 from the NOAA web site <http://www.esrl.noaa.gov/psd/repository/alias/facts/>
373 were crucial to this analysis. This work was supported by NSF grant AGS-0960497.

374 The author gratefully acknowledges colleagues, Nick Bond, Paulo Ceppi, Greg
375 Johnson, Todd Mitchell, Richard Seager, LuAnne Thompson, and Mike Wallace,
376 whose generous advice and comments greatly improved this contribution. The
377 comments of two anonymous reviewers of an earlier version of this work were
378 extremely helpful.

379

380

381 **References:**

382

383 Alexander, M. A., I. Blade, M. Newman, J. R. Lanzante, N. C. Lau, and J. D. Scott (2002),

384 The atmospheric bridge: The influence of ENSO teleconnections on air-sea

385 interaction over the global oceans, *J. Climate*, 15(16), 2205-2231.

386 Barnes, E. A. (2013), Revisiting the evidence linking Arctic amplification to extreme

387 weather in midlatitudes, *Geophys. Res. Lett.*, 40(17), 4734-4739.

388 Barsugli, J. J., and D. S. Battisti (1998), The basic effects of atmosphere-ocean

389 thermal coupling on midlatitude variability, *J. Atmos. Sci.*, 55(4), 477-493.

390 Blunden, J., and D. S. Arndt (2014), State of the Climate in 2013, *Bull. Amer. Meteorol.*

391 *Soc.*, 95(7), S1-S257.

392 Bond, N. A., J. E. Overland, M. Spillane, and P. Stabeno (2003), Recent shifts in the

393 state of the North Pacific, *Geophys. Res. Lett.*, 30(23),

394 doi:10.1029/2003gl018597.

395 Bretherton, C. S., M. Widmann, V. P. Dymnikov, J. M. Wallace, and I. Blade (1999), The
396 effective number of spatial degrees of freedom of a time-varying field, *J.*
397 *Climate*, 12(JUL 1999), 1990-2009.

398 Cayan, D. R. (1992), Latent and sensible heat flux anomalies over the northern
399 oceans: The connection to monthly atmospheric circulation, *J. Climate*, 5,
400 354-369.

401 Ceballos, L. I., E. Di Lorenzo, C. D. Hoyos, N. Schneider, and B. Taguchi (2009), North
402 Pacific Gyre Oscillation Synchronizes Climate Fluctuations in the Eastern and
403 Western Boundary Systems, *J. Climate*, 22(19), 5163-5174,
404 doi:5110.1175/2009jcli2848.5161.

405 Chhak, K. C., E. Di Lorenzo, N. Schneider, and P. F. Cummins (2009), Forcing of Low-
406 Frequency Ocean Variability in the Northeast Pacific, *J. Climate*, 22(5), 1255-
407 1276, doi:1210.1175/2008jcli2639.1251.

408 Compo, G. P., et al. (2011), The Twentieth Century Reanalysis Project, *Quart. J. Royal*
409 *Meteorol. Soc.*, 137(654), 1-28, doi; 10.1002/qj.1776.

410 Cummins, P. F., and H. J. Freeland (2007), Variability of the North Pacific current and
411 its bifurcation, *Progr. Oceanography*, 75(2), 253-265, doi:
412 210.1016/j.pocean.2007.1008.1006.

413 Davis, R. E. (1976), Predictability of sea-surface temperature and sea-level pressure
414 anomalies over the North Pacific Ocean, *J. Phys. Ocean.*, 6(3), 249-266.

415 Deser, C., and M. L. Blackmon (1995), On the relationship between tropical and
416 North Pacific Sea-Surface Temperature Variations, *J. Climate*, 8(6), 1677-
417 1680.

418 Deser, C., A. Phillips, V. Bourdette, and H. Y. Teng (2012), Uncertainty in climate
419 change projections: the role of internal variability, *Clim. Dyn.*, 38(3-4), 527-
420 546, doi:510.1007/s00382-00010-00977-x.

421 Di Lorenzo, E., et al. (2008), North Pacific Gyre Oscillation links ocean climate and
422 ecosystem change, *Geophys. Res. Lett.*, 35(8), doi: 10.1029/2007gl032838.

423 Ding, Q. H., J. M. Wallace, D. S. Battisti, E. J. Steig, A. J. E. Gallant, H. J. Kim, and L. Geng
424 (2014), Tropical forcing of the recent rapid Arctic warming in northeastern
425 Canada and Greenland, *Nature*, 509(7499), doi 10.1038/nature13260.

426 Eade, R., D. Smith, A. Scaife, E. Wallace, N. Dunstone, L. Hermanson, and N. Robinson
427 (2014), Do seasonal-to-decadal climate predictions underestimate the
428 predictability of the real world?, *Geophys. Res. Lett.*, 41(15), 5620-5628,
429 doi:5610.1002/2014gl061146.

430 Francis, J. A., and S. J. Vavrus (2012), Evidence linking Arctic amplification to
431 extreme weather in mid-latitudes, *Geophys. Res. Lett.*, 39,
432 doi:10.1029/2012gl051000.

433 Frankignoul, C., N. Sennechael, Y. O. Kwon, and M. A. Alexander (2011), Influence of
434 the Meridional Shifts of the Kuroshio and the Oyashio Extensions on the
435 Atmospheric Circulation, *J. Climate*, 24(3), 762-777.

436 Horel, J. D., and J. M. Wallace (1981), Planetary-scale atmospheric phenomena
437 associated with the Southern Oscillation, *Mon. Wea. Rev.*, 109, 813-829.

438 Huber, M., and R. Knutti (2014), Natural variability, radiative forcing and climate
439 response in the recent hiatus reconciled, *Nature Geosci.*, 7(9), 651-656,
440 doi:610.1038/ngeo2228.

441 Kalnay, E., et al. (1996), The NCEP/NCAR 40-year Reanalysis Project, *Bull. Amer.*
442 *Meteor. Soc.*, 77(March), 437-471.

443 Kim, B.-M., S.-W. Son, S.-K. Min, J.-H. Jeong, S.-J. Kim, X. Zhang, T. Shim, and J.-H. Yoon
444 (2014), Weakening of the stratospheric polar vortex by Arctic sea-ice loss,
445 *Nature Com.*, 5, doi:10.1038/ncomms5646.

446 Kosaka, Y., and S. P. Xie (2013), Recent global-warming hiatus tied to equatorial
447 Pacific surface cooling, *Nature*, 501(7467), doi 10.1038/nature12534.

448 Kushnir, Y., W. A. Robinson, I. Blade, N. M. J. Hall, S. Peng, and R. Sutton (2002),
449 Atmospheric GCM response to extratropical SST anomalies: Synthesis and
450 evaluation, *J. Climate*, 15(16), 2233-2256.

451 Kwon, Y. O., M. A. Alexander, N. A. Bond, C. Frankignoul, H. Nakamura, B. Qiu, and L.
452 Thompson (2010), Role of the Gulf Stream and Kuroshio-Oyashio Systems in
453 Large-Scale Atmosphere-Ocean Interaction: A Review, *J. Climate*, 23(12),
454 3249-3281.

455 Lau, N. C., and M. J. Nath (1994), A Modeling Study of the Relative Roles of Tropical
456 and Extratropical Sst Anomalies in the Variability of the Global Atmosphere
457 Ocean System, *J. Climate*, 7(8), 1184-1207.

458 Lau, N. C., and M. J. Nath (1996), The role of the "atmospheric bridge" in linking
459 tropical Pacific ENSO events to extratropical SST anomalies, *J. Climate*, 9(9),
460 2036-2057.

461 Liu, Z. Y., and M. Alexander (2007), Atmospheric bridge, oceanic tunnel, and global
462 climatic teleconnections, *Rev. Geophys.*, 45(2), doi 10.1029/2005RG000172.

463 Mantua, N. J., and S. R. Hare (2002), The Pacific decadal oscillation, *J. Oceanography*,
464 58(1), 35-44.

465 Mantua, N. J., S. R. Hare, Y. Zhang, J. M. Wallace, and R. C. Francis (1997), A Pacific
466 interdecadal climate oscillation with impacts on salmon production, *Bull.*
467 *Amer. Meteorolog. Soc.*, 78(6), 1069-1079.

468 Miller, A. J., D. R. Cayan, and W. B. White (1998), A westward-intensified decadal
469 change in the North Pacific thermocline and gyre-scale circulation, *J. Climate*,
470 11(12), 3112-3127.

471 Neelin, J. D., D. S. Battisti, A. C. Hirst, F.-J. Fei, Y. Wakata, T. Yamagata, and S. E. Zebiak
472 (1998), ENSO theory, *J. Geophys. Res.*, 103(C7), 14261-14290.

473 Newlin, M. L., and M. C. Gregg (2014), Global Oceans [in “State of the Climate in
474 2013”], *Bull. Amer. Meteor. Soc.*, 95(7), S51–S78.

475 North, G. T., Bell, R. Cahalan, and F. Moeng (1982), Sampling errors in the estimation
476 of empirical orthogonal functions, *Mon. Wea. Rev.*, 110, 699-706.

477 Palmer, T. N., and D. L. T. Anderson (1994), The prospects for seasonal forecasting-a
478 review paper, *Quart. J. Roy. Meteorol. Soc.*, 120(518), 755-793.

479 Qiu, B. (2000), Interannual variability of the Kuroshio Extension system and its
480 impact on the wintertime SST field, *J. Phys. Ocean.*, 30(6), 1486-1502.

481 Rasmusson, E. M., and J. M. Wallace (1983), Meteorological aspects of the El
482 Niño/Southern Oscillation., *Science*, 222, 1195-1202.

483 Rayner, N. A., D. E. Parker, E. B. Horton, C. K. Folland, L. V. Alexander, D. P. Rowell, E.
484 C. Kent, and A. Kaplan (2003), Global analyses of sea surface temperature, sea

485 ice, and night marine air temperature since the late nineteenth century, *J.*
486 *Geophys. Re.-Atmos.*, 108(D14), doi10.1029/2002jd002670.

487 Seager, R., and M. Hoerling (2014), Atmosphere and Ocean Origins of North
488 American Droughts, *J. Climate*, 27(12), 4581-4606.

489 Seager, R., Y. Kushnir, N. H. Naik, M. A. Cane, and J. Miller (2001), Wind-driven shifts
490 in the latitude of the Kuroshio-Oyashio Extension and generation of SST
491 anomalies on decadal timescales, *J. Climate*, 14(2001), 4249-4265.

492 Seager, R., M. Hoerling, S. Schubert, H. Wang, B. Lyon, A. Kumar, J. Nakamura, and N.
493 Henderson (2014), Causes and Predicatability of the 2011-14 California
494 Drought, *Rep.*, doi:10.7289/V7258K7771F, 40pp.

495 Smirnov, D., M. Newman, and M. A. Alexander (2014), Investigating the Role of
496 Ocean-Atmosphere Coupling in the North Pacific Ocean, *J. Climate*, 27(2),
497 592-606.

498 Smith, T. M., R. W. Reynolds, T. C. Peterson, and J. Lawrimore (2008), Improvements
499 to NOAA's historical merged land-ocean surface temperature analysis (1880-
500 2006), *J. Climate*, 21(10), 2283-2296.

501 Trenberth, K. E., and J. T. Fasullo (2013), An apparent hiatus in global warming?,
502 *Earth's Future*, 1(1), 19-32.

503 Vimont, D. J., D. S. Battisti, and A. C. Hirst (2001), Footprinting: A seasonal
504 connection between the tropics and mid-latitudes, *Geophys. Res. Lett.*, 28(20),
505 3923-3926.

506 Vimont, D. J., J. M. Wallace, and D. S. Battisti (2003), The seasonal footprinting
507 mechanism in the Pacific: Implications for ENSO, *J. Climate*, 16(16), 2668-
508 2675.

509 Vivier, F., K. A. Kelly, and L. Thompson (1999), Contributions of wind forcing, waves,
510 and surface heating to sea surface height observations in the Pacific Ocean,
511 *J. Geophys. Res.-Oceans*, 104(C9), 20767-20788.

512 Wang, F. Y., Z. Y. Liu, and M. Notaro (2013), Extracting the Dominant SST Modes
513 Impacting North America's Observed Climate, *J. Climate*, 26(15), 5434-5452,
514 doi: 5410.1175/jcli-d-5412-00583.00581.

515 Wang, S. Y., L. Hipps, R. R. Gillies, and J.-H. Yoon (2014), Probable causes of the
516 abnormal ridge accompanying the 2013–2014 California drought: ENSO
517 precursor and anthropogenic warming footprint, *Geophys. Res. Lett.*, 41(9),
518 doi:10.1002/2014GL059748.

519 Zhang, Y., J. M. Wallace, and D. S. Battisti (1997), ENSO-like interdecadal variability:
520 1900-93, *J. Climate*, 10(5), 1004-1020.

521

522

523

524 **Figure Captions:**

525

526 Fig. 1 The regressions of monthly mean anomalies of global SST onto the first three
527 EOFs of SST for the ocean area 30S-65N, 120E-105W and the period from January
528 1900 to July 2014. Contour interval is 0.1°C. Positive values are red, negative values
529 are blue, and the zero contour is white. Robinson Projection from 60S-60N.

530

531 Fig. 2 Time series of the Principal Components of the first three EOFs of monthly
532 mean Pacific SST poleward of 30S as shown in Fig. 1. Only values from January 1979
533 to January of 2015 are shown. Units are standard deviations. Values are offset by
534 four standard deviations for clearer viewing.

535

536 Fig. 3 (a) The observed anomaly in 500hPa height for November 2013 to March
537 2014 (contour interval is 10m, positive is red, negative is blue and the zero contour
538 is white). (b) Regression of the 500hPa height anomalies for the months of
539 November to March for the years from 1979-2014 onto the principal component
540 time series for the second EOF of global SST for the period from 1979 to 2014.
541 (contour interval is 3m) (c) Same as b, except that the height data is from the 50-
542 member ensemble from the ESRL-GFSv2 using the observed SST.

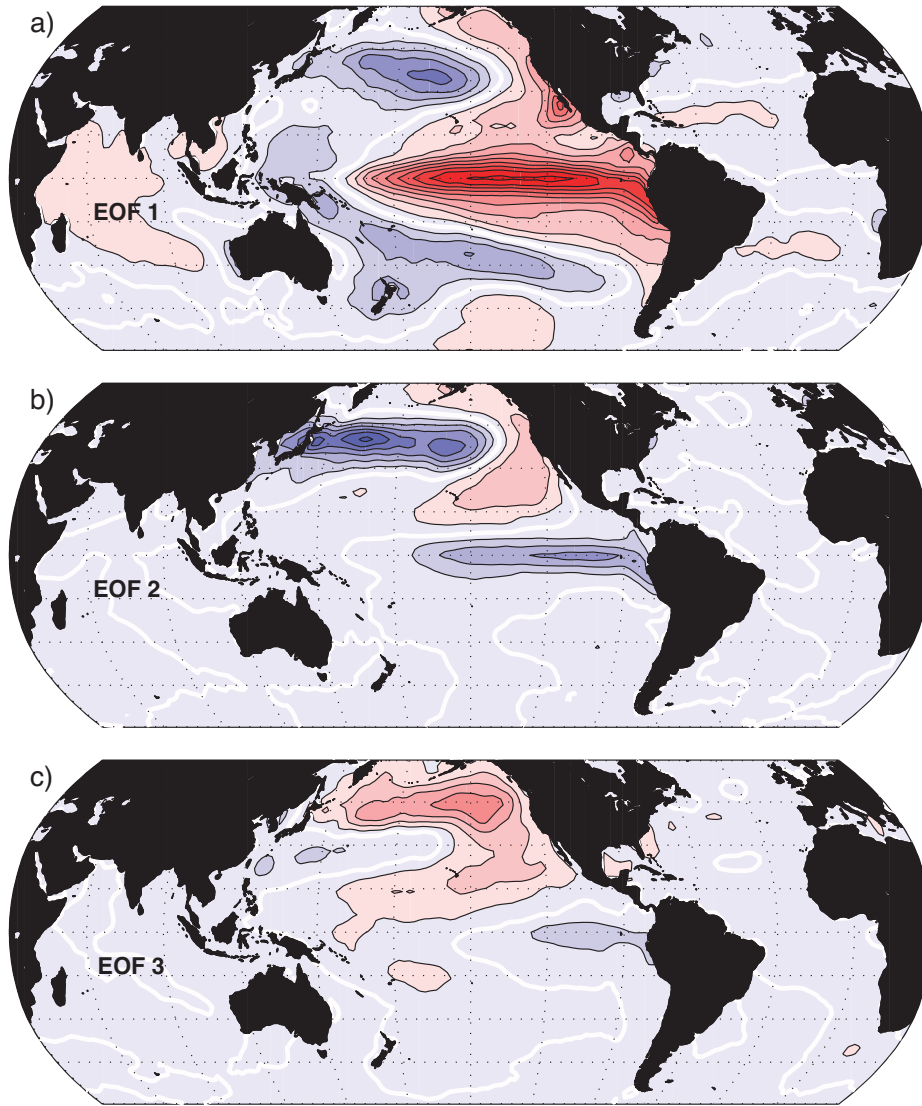
543

544 Fig. 4 the same as Fig. 3, except that the variable plotted is the temperature at the
545 lowest model level. Contour interval is 0.5 in a) and 0.1 in b) and c).

546

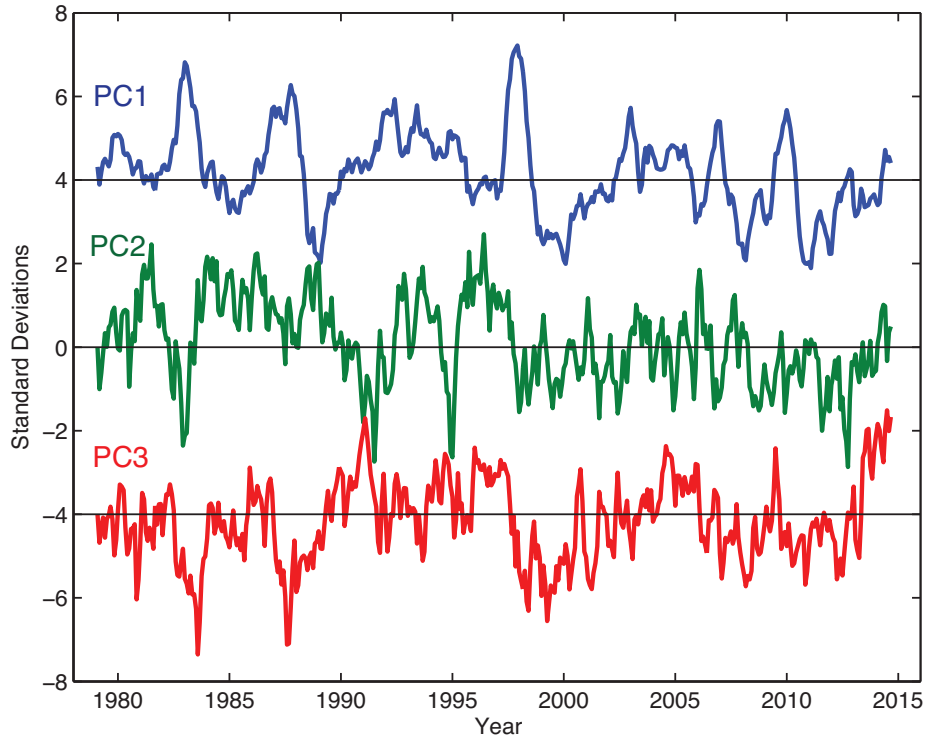
547
548
549
550

Figures to go with: "Pacific Sea Surface Temperature and the Winter of 2014"



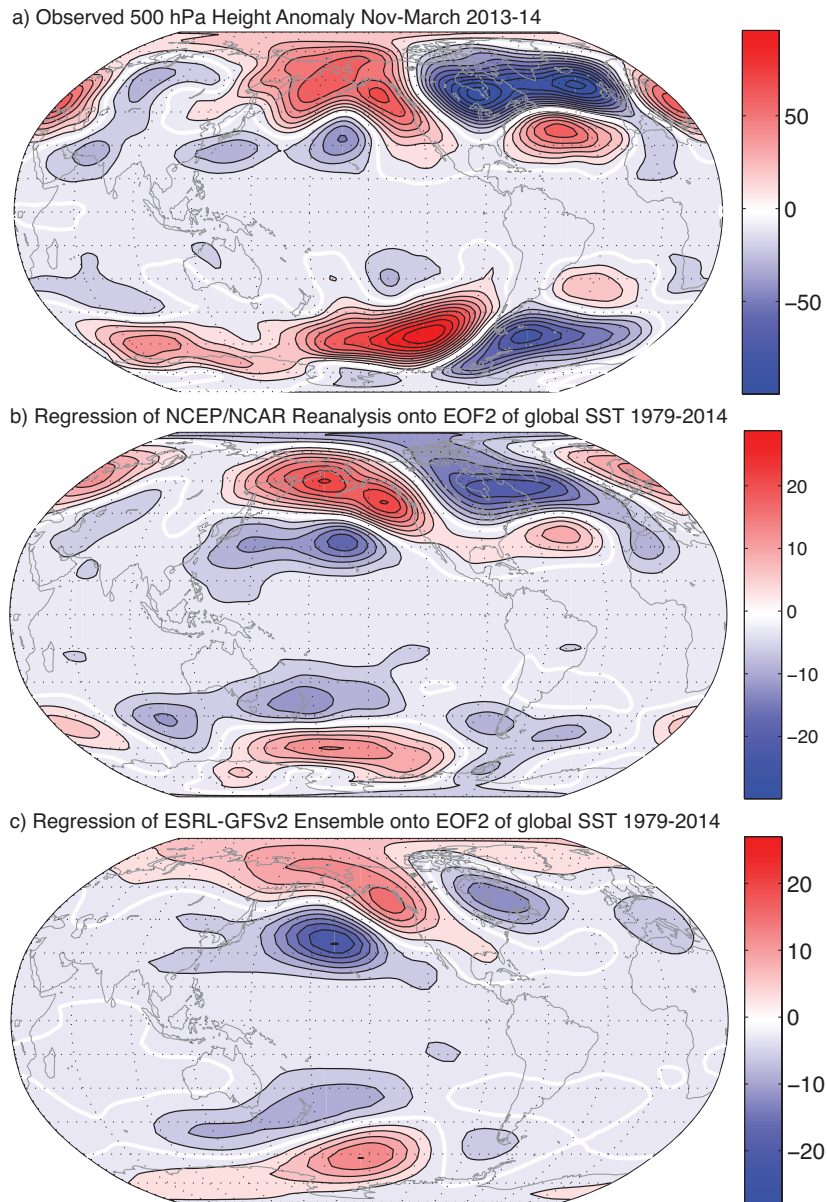
551
552
553
554
555
556
557

Fig. 1 The regressions of monthly mean anomalies of global SST onto the first three EOFs of SST for the ocean area 30S-65N, 120E-105W and the period from January 1900 to July 2014. Contour interval is 0.1°C. Positive values are red, negative values are blue, and the zero contour is white. Robinson Projection from 60S-60N.



558
559
560
561
562
563
564
565

Fig. 2 Time series of the Principal Components of the first three EOFs of monthly mean Pacific SST poleward of 30S as shown in Fig. 1. Only values from January 1979 to January of 2015 are shown. Units are standard deviations. Values are offset by four standard deviations for clearer viewing.



566

567

568 Fig. 3 (a) The observed anomaly in 500hPa height for November 2013 to March

569 2014 (contour interval is 10m, positive is red and negative is blue and zero contour

570 is white). (b) Regression of the 500hPa height anomalies for the months of

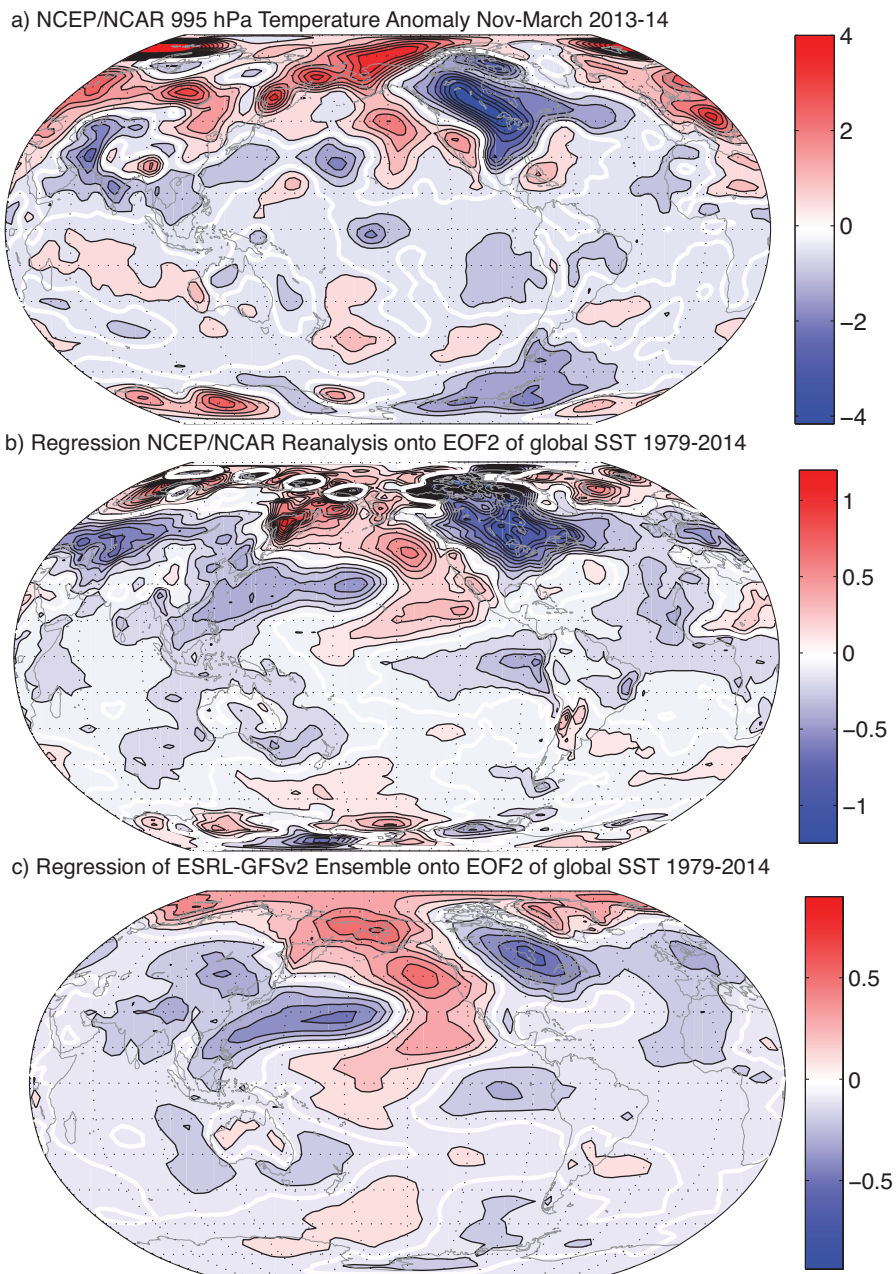
571 November to March for the years from 1979-2014 onto the principal component

572 time series for the second EOF of global SST for the period from 1979 to 2014.

573 (contour interval is 3m) (c) Same as b, except that the height data is from the 50-

574 member ensemble from the ESRL-GFSv2 using the observed SST.

575



576

577

578 Fig. 4 the same as Fig. 3, except that the variable plotted is the temperature at the

579 lowest model level. Contour interval is 0.5 in a) and 0.1 in b) and c).

Supplementary Material for
Pacific Sea Surface Temperature and the Winter of 2014

Dennis L. Hartmann¹

Corresponding Author: Dennis L. Hartmann, Department of Atmospheric Sciences,
Box 351640, University of Washington, Seattle, Washington 98195

These figures supplement those in the published paper.

Fig. S1 shows the eigenvalue spectrum for the analysis of the Pacific Ocean from 30S to 65N for the period from 1900 to 2014. The first mode is ENSO, explains about 30% of the variance and is well separated from the other modes by the North et al. [1982] criterion. The second and third modes explain about 8% each and are separated from the rest of the modes, but are not distinct from each other by the explained variance criterion. The regression patterns for these modes are shown in Fig. 1.

Fig. S2 shows the lagged autocorrelation and the lagged cross correlation for the principal components of the first three modes in Fig. S1 and Fig. 1. The lagged autocorrelations in the top show that the ENSO mode (PC1) has a quasi-periodic

¹ Department of Atmospheric Sciences, University of Washington,
Seattle, Washington 98195

behavior with a characteristic time of two or more years. The second and third modes have almost identical autocorrelations that have a shoulder around a lag of 12 months. These are decadal modes with a lot of red noise, but significant year-to-year memory. The autocorrelations for the decadal modes fall off rapidly at first, but then have more autocorrelation at 12 months lag than ENSO. The rapid falloff of the autocorrelation of the decadal modes may result from random forcing from the atmosphere, which tends to give the autocorrelation an exponential structure, like that of red noise. Underlying this is some strong correlation at interannual time scales, perhaps related to the reemergence of heat content anomalies laid down in previous winters, or from ocean dynamics with time scales of a year or longer.

The bottom panel of Fig. S2 shows the lagged cross correlations between the first three modes. The second mode, with cold extratropical SSTs in the same region where ENSO produces cold SSTs, lags behind the ENSO mode, with significant positive correlations a year or so after an ENSO warm event. This may result from the atmospheric bridge mechanism, whereby tropical SST anomalies associated with ENSO send off atmospheric Rossby Waves that modulate the ocean heat content in the extratropics, especially during winter. These extratropical anomalies persist longer than the equatorial anomalies with which they are associated. The third mode has positive correlations preceding the ENSO mode, so that warm SST anomalies in the subtropical and extratropical East Pacific precede warm ENSO events. This latter behavior corresponds to the 'footprinting' mechanism described by Vimont et al. [Vimont et al., 2001; Vimont et al., 2003].

Fig. S3 shows the correlation of the 500hPa height with the principal components of the first three modes of Pacific SST based on the 1900-2014 period. The first mode has a strong tropical mean correlation, as well as a wave structure that starts in the deep Tropics. The decadal modes have weaker connections to the deep Tropics, but the third EOF (NPM) has a slightly negative correlation with the tropical mean height. In the extratropics and over North America the correlations of height with the three SST modes are comparable.

Fig. S4 shows the regressions of the 500hPa height anomalies from the ensemble average AMIP experiments onto the principal component time series of the third EOF of Pacific SST (NPM) as in Fig. 4c, but showing the results for all three models available from the NOAA web site. All model ensembles produce similar regression patterns that result from the specification of the observed SST under these models. Thus the SST anomalies are acting to produce 500hPa anomaly patterns that look like that in 2014.

Fig. S5 shows the simulation of the 2013-14 winter anomalies by the ESRL-GFSv2 50-member ensemble. The features over North America in the observations in Figs. 3 and 4 are very much under-represented. The near-surface temperature in particular is poorly simulated, with warming spreading downstream from the North Pacific Ocean warm anomaly, and the cold anomaly very weak and displaced toward the east. This echoes the somewhat weak regressions in Fig. 4c.

Supplementary Figures

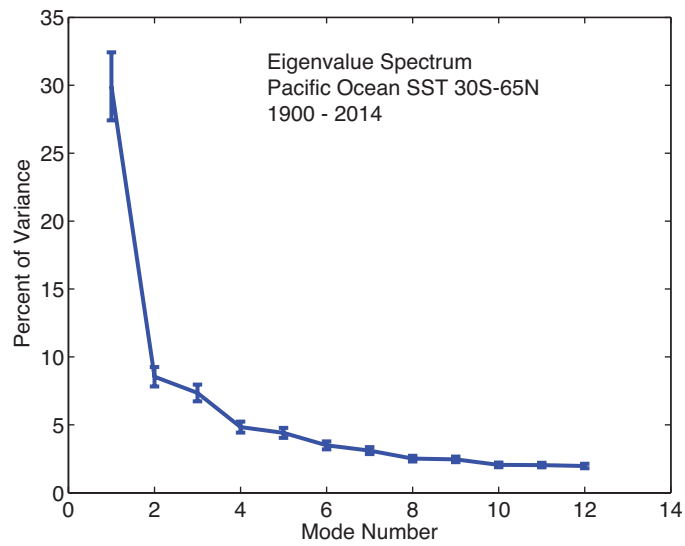


Fig. S1 Eigenvalue spectrum with 95% confidence intervals for Pacific Ocean SST from 30S to 65N for the period from 1900 to 2014. Spatial structures corresponding to these eigenvalues are shown in Fig. 1.

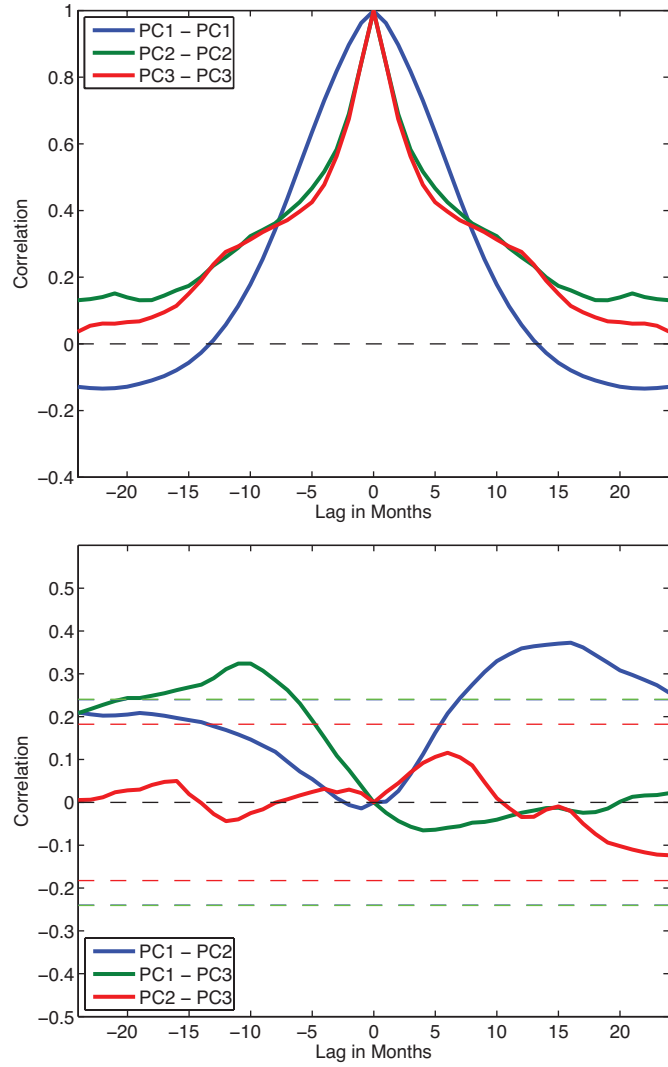


Fig. S2 (top) Lagged autocorrelation of the principal components of the first three EOFs of SST from 30S to 65N in the Pacific for the period from 1950-2014. (bottom) lagged cross-correlations for the first three principal components. 95% significance levels are indicated with the dashed lines.

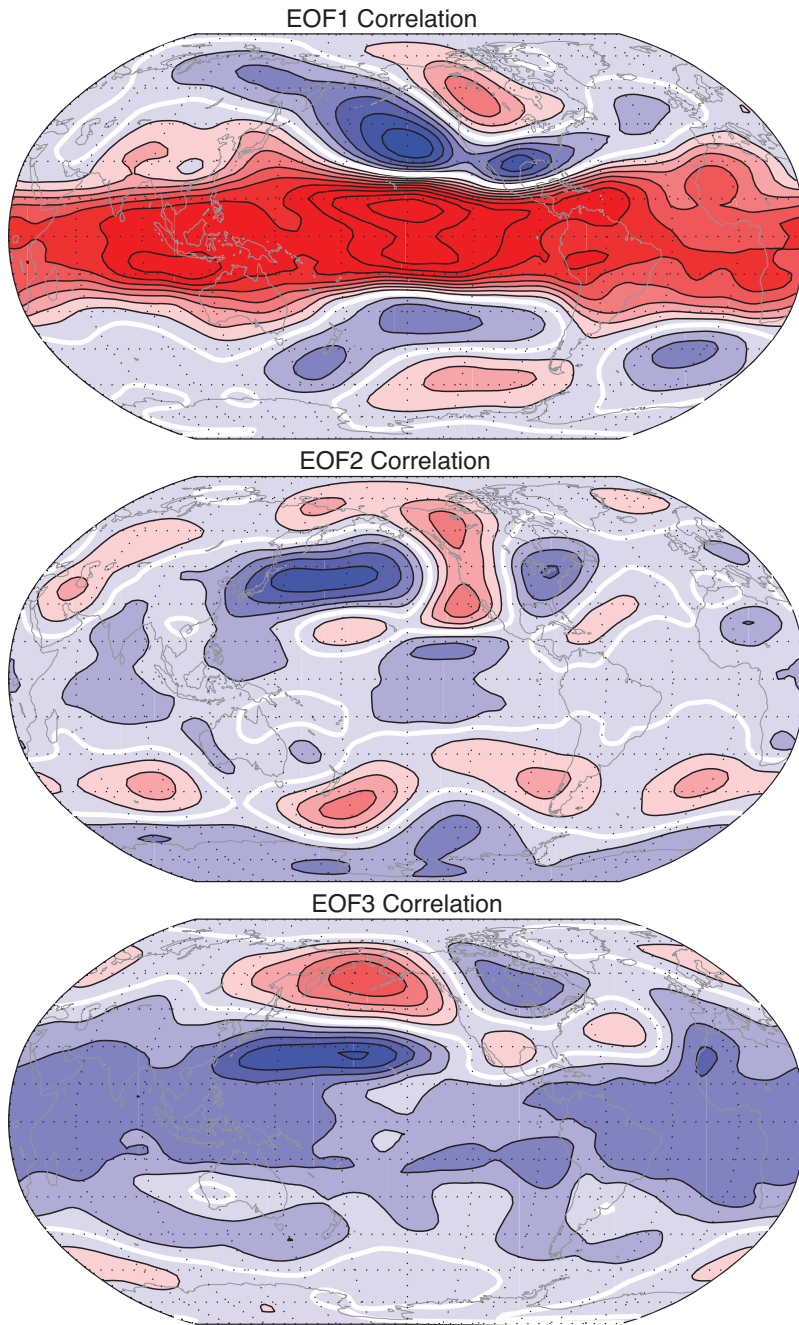
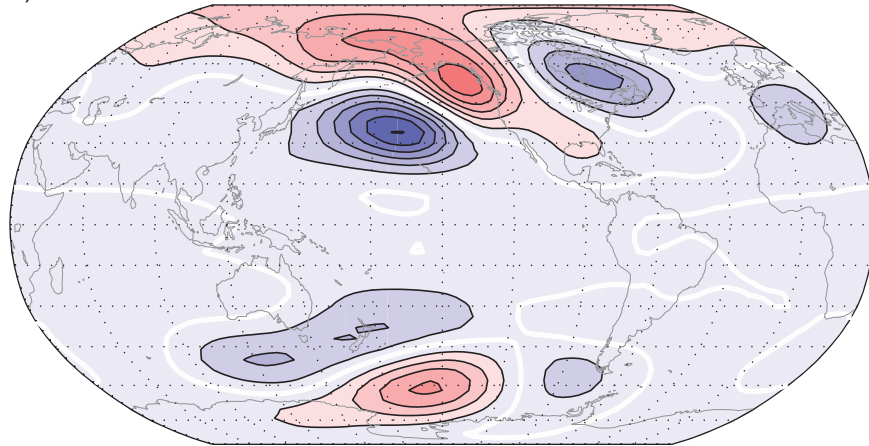
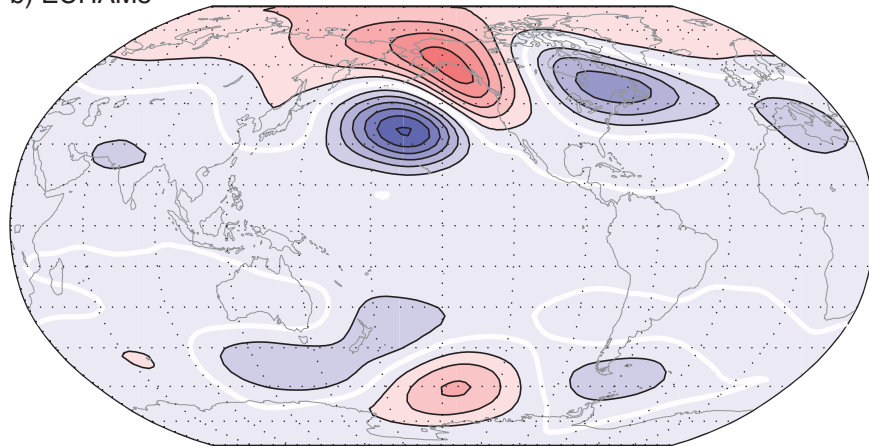


Fig. S3 Correlations of the 500hPa height field during November through March from NCEP/NCAR reanalysis since 1948 with the principle components of the first three EOFs of Pacific Ocean SST determined for the period since 1900. Contours are 0.1 and the zero correlation line is white. Correlations bigger than about 0.2 are significant at 95%.

a) ESRL-GFSv2



b) ECHAM5



c) CAM4

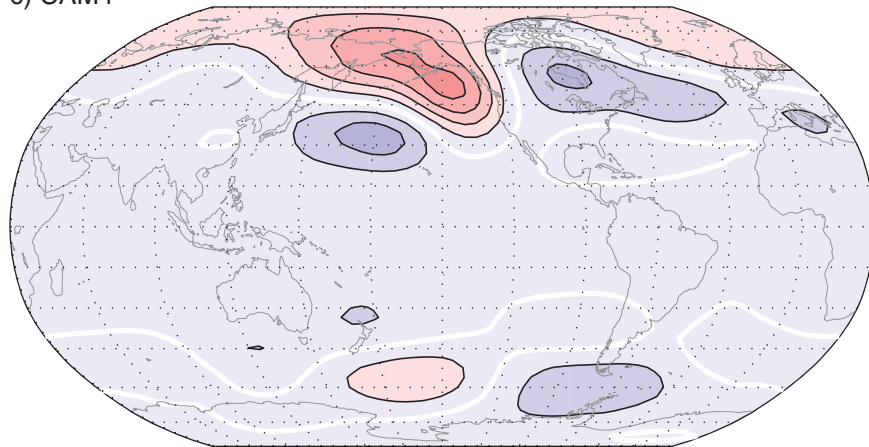
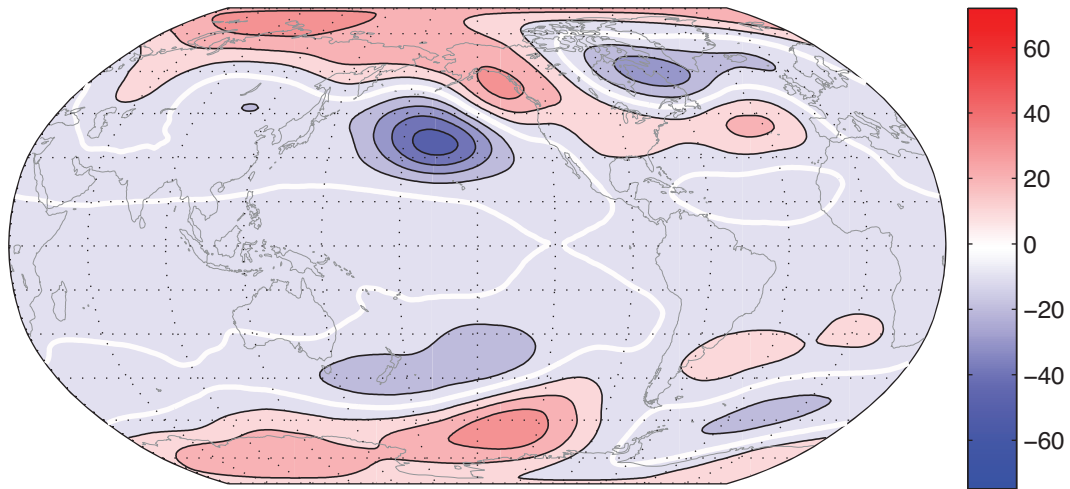


Fig. S4 Regression of the 500hPa height onto the principal component of the third EOF of SST as in Fig. 4 bottom, but also showing the results from the ECHAM5 and CAM4 ensemble means. Contour interval is 3m, and the zero contour is white.

a) ESRL-GFSv2 simulation of NDJFM 2013-14 500hPa Height Anomaly



b) ESRL-GFSv2 simulation of NDJFM 2013-14 1000hPa Temperature Anomaly

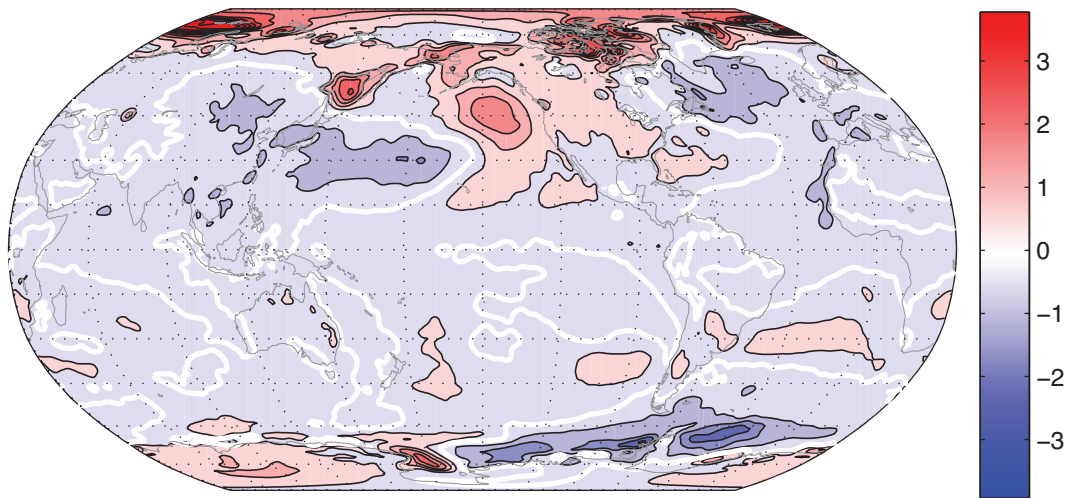


Fig. S5 Simulation of the winter of November to March 2013-14 anomaly of the a) 500hPa height (contour interval 10m) and b) 1000 hPa temperature (contour interval 0.5K) by the 50-member ensemble mean of the ESRL-GFSv2 model.

References

- North, G. T., Bell, R. Cahalan, and F. Moeng (1982), Sampling errors in the estimation of empirical orthogonal functions, *Mon. Wea. Rev.*, *110*, 699-706.
- Vimont, D. J., D. S. Battisti, and A. C. Hirst (2001), Footprinting: A seasonal connection between the tropics and mid-latitudes, *Geophys. Res. Lett.*, *28*(20), 3923-3926.
- Vimont, D. J., J. M. Wallace, and D. S. Battisti (2003), The seasonal footprinting mechanism in the Pacific: Implications for ENSO, *J. Climate*, *16*(16), 2668-2675.